ARTICLE

WILEY

"Third-body" collision parameters for hydrocarbons, alcohols, and hydroperoxides and an effective internal rotor approach for estimating them

Ahren W. Jasper [iD]

Chemical Sciences and Engineering Division, Argonne National Laboratory, Lemont, Illinois

Correspondence

Ahren W. Jasper, Chemical Sciences and Engineering Division, Argonne National Laboratory, Lemont, IL 60439.
Email: ajasper@anl.gov

Abstract

Collision rate constants and third-body collision efficiencies are calculated for more than 300 alkanes, alcohols, and hydroperoxides, for the bath gases He, Ar, H_2, and N_2, and from 300 to 2000 K. The data set includes highly branched species and species with as many as 16 nonhydrogen atoms N, and it is analyzed to develop strategies for estimating collision properties more generally. Simple analytic formulas describing the Lennard-Jones collision parameters σ and ε are obtained for each of the three classes of systems as a function of N. Trends in the collision efficiency range parameter $\alpha = \langle \Delta E_d \rangle$ are more complicated, and a method is developed and validated for estimating α based on the numbers and types of internal rotors and oxygen-containing groups. Specifically, the approach maps the expected value of α for a branched alkane, alcohol, or hydroperoxide onto those for the corresponding normal (linear) series via an effective number of nonhydrogen atoms N_{eff}. The prescription for N_{eff} is based on counting internal rotor types and is shown to be insensitive to temperature and fairly insensitive to the identity of the bath gas. Together, these strategies allow for the ready estimation of the collision parameters σ, ε, and α so long as results for the associated linear series are available.

KEYWORDS

classical trajectories, Lennard-Jones parameters, third-body collision efficiencies, unimolecular kinetics, automation

1 | INTRODUCTION

Detailed chemical kinetic models are comprised of (nowadays, often quite extensive) parameter databases describing elementary reaction rates, thermochemistry, and transport.[1–9] The role of a priori theory as an independent source of information for populating these databases and for improving the models they reflect continues to increase.[10–13]

Here, we consider a priori theoretical approaches for computing collision rate constants and efficiencies relevant to the prediction of transport properties[14–16] and pressure dependence in elementary kinetics.[17–20] These phenomena are controlled by so-called "third-body" bath gas collisions,

and we recently used trajectory-based collision parameters to compute diffusion coefficients[21] and pressure-dependent kinetics[22] with accuracies comparable to those from experiment. Our predictive work benefitted from a long history of combustion-relevant trajectory studies of collisional energy transfer (see, eg, Refs. 23–32 and the recent review from Lendvay[33]) as well as quantum mechanical scattering predictions of transport properties,[34–37] and it is similar to ongoing work from several groups (eg, Refs. 38–41).

Collisional activation is the dynamical bottleneck in the low-pressure limit of a unimolecular reaction, A (+M) = B + C (+M), where the reaction rate $k_{0,M}$[A][M] depends linearly on pressure. Chemical kinetics tabulations sometimes include

$k_{0,M}$ for a reference bath gas (eg, Ar) along with relative collision efficiencies (expressed as ratios of $k_{0,M}$) for other baths, but for many reactions this information is not available. More generally and despite some systematic experimental studies (eg, Refs. 42–54), it remains difficult to anticipate how collision efficiencies vary with the temperature and identity of the bath gas M as well as the size and chemical structure of the unimolecular reactant A.

We do know that the rate constants $k_{0,M}$ can vary significantly for different bath gases M and that their relative efficiencies are temperature dependent. As examples we highlight a few experimental studies from Michael and co-workers. In a series of papers from the 1970s,[42–44] $k_{0,M}$ was shown to vary by as much as factor of four even among the so-called "weak" colliders (eg, M = He, Ar, Kr, H_2, N_2, O_2), while more recently[50] the important combustion reaction H + O_2 (+M) was shown to be ~25× faster for the strong collider M = H_2O than for M = Ar.

The goal of the present work is to use trajectory-based predictions of collisional energy transfer to develop rules for describing how the collision parameters that control $k_{0,M}$ depend on the size, composition, and structure of A. Specifically, we consider a total of 307 unimolecular reactants A with as many as 16 nonhydrogen ("heavy") atoms N, including alcohols, hydroperoxides, and highly branched hydrocarbons, and the baths M = He, Ar, H_2, and N_2.

The present work considerably extends our previous study[55] where 38 hydrocarbons with N = 1-8 were studied for seven baths, M = He, Ne, Ar, Kr, H_2, N_2, and O_2. Collision parameters were found to be quite similar for M = Ar and Kr and for N_2 and O_2, and we therefore exclude Kr and O_2 from consideration here along with Ne, which is less commonly needed in combustion database compilations. Important baths like M = H_2O and CO_2 are also not considered, as these baths require complex strategies for accurately representing their A + M interaction potentials that complicate the consideration of large numbers of systems.[56]

The large data set generated here is analyzed to develop and validate simple expressions for estimating the Lennard-Jones collision parameters σ and ε as well as a commonly used measure of the collision efficiency $\alpha = \langle \Delta E_d \rangle$, which is the average energy transferred in deactivating collisions. We show that α can be reliably estimated using an "effective" number of nonhydrogen atoms N_{eff}, which is determined simply by counting the numbers and types of internal rotors (eg, torsions) in A.

This paper is organized as follows: In Section 2, we briefly summarize the strategies used here for potential energy surface (PES) construction, for computing the Lennard-Jones parameters σ and ε, and for preparing and analyzing the trajectories used to compute α. We also outline a general automation strategy that enabled the more than 11 million trajectories that were needed for this work. Section 3 includes a brief test of

our choice of molecular mechanics force field for describing A. Then, the systematic parameterization of N_{eff} is described using data for 1000 K and M = Ar. The resulting prescriptions for N_{eff} are subsequently tested and validated using the full data set, including data obtained at 300 and 2000 K and for M = He, H_2, and N_2. Section 4 is a conclusion.

2 | THEORY

2.1 | Potential energy surfaces

PESs describing A + M collisions are a prerequisite for predicting collision parameters, and we have previously used a simple transferable "separable and pairwise" approach for constructing them.[57] Similar approaches have a long history of use in trajectory studies of collisional energy transfer (eg, Refs. 58–61). Briefly, pairwise Buckingham (exp/6) interactions were parameterized against calculated ab initio interaction energies for a reference system (CH_4 + M). The resulting interaction parameters were assumed to be transferable to larger C_xH_y + M systems, and the good accuracy of this assumption was demonstrated.[55,56] This approach greatly simplifies the consideration of large numbers of systems, as required here.

For C_xH_y + He, Ar, H_2, and N_2, and $C_xH_{2x+1}OH$ + He and Ar, we used our previously developed exp/6 parametrizations.[56,57] New exp/6 PESs were generated for this work to describe $C_xH_{2x+1}OOH$ + He and Ar using the same electronic structure theory, sampling, and fitting strategies that were used for alcohols in Ref. 56. The new $C_xH_{2x+1}OOH$ + He and Ar parameterizations and comparisons of the ab initio and fitted energies are included as the Supporting Information. As noted in Ref. 56, the separable and pairwise exp/6 approach is not accurate when the interaction potential is too anisotropic, such as for alcohols and M = N_2. Therefore, diatomic baths were not considered here for any oxygenated species A.

In the present work, the species A are common organic molecules, and A + M collisions are always nonreactive. We therefore used molecular mechanics force fields for describing the intramolecular PES of A. Specifically, the Tinker software package[62] was used, and we tested three related force fields distributed with it: MM3,[63] AMBER,[64] and OPLS.[65] A tight binding (TB) model for hydrocarbons was also tested.[66] As shown below, we find only small differences in the results obtained using the different force fields, and unless otherwise indicated the present results were obtained using MM3.

2.2 | The Lennard-Jones parameters σ and ε

As described in a recent review,[15] transport databases typically consist of pairs of Lennard-Jones parameters (the well

depth ε and collision diameter σ) describing self-collisions (ie, A + A collisions) for every species of interest. Combining rules are employed to generate the required binary (ie, A + M) collision parameters (typically via geometric and arithmetic averages for ε and σ, respectively), and these are converted to transport properties and collision rates via isotropic 12/6 Lennard-Jones formulas.

In addition to errors associated with the use of simple combining rules, the 12/6 Lennard-Jones model ignores anisotropy in the intermolecular PES, the internal coordinates of the colliders, and the softness of the repulsive wall. While these errors can be important,[21] particularly the error associated with the treatment of the repulsive wall,[16,36] incorporating more detailed transport models into existing kinetics codes and databases remains rare. We therefore limit attention to the prediction of the collision parameters ε and σ, despite the simplifications they represent.

We computed the collision parameters σ and ε using the "one-dimensional minimizations" method[67] and the distributed code 1DMIN.[68] In this approach, the inner turning point at the energy of the asymptote and the minimum energy of the interaction potential at several fixed orientations are averaged to determine σ and ε, respectively. Aside from special cases like A = H and H_2, which are not considered here, the use of these effective isotropic 12/6 Lennard-Jones parameters is not likely a significant source of error for transport and collision rate calculations in combustion, as previously quantified via comparisons with "exact" classical trajectory results[21] and with tabulated values.[67]

2.3 | The collision efficiency range parameter α

Detailed models for the collisional energy transfer function[22,38] have been shown to enable a priori kinetics predictions with errors of just 25%,[22,69] whereas simpler models that incorporate fewer physical details, such as the "single-exponential-down" model[17,45] that is often used in energy-resolved master equation calculations,[70–72] have a priori accuracies of closer to a factor of two.[69,73–75] Again, in an effort to be most directly useful for constructing extensive chemical kinetics tabulations, we restrict attention to models where collision outcomes are controlled by the single parameter $\alpha = \langle \Delta E_d \rangle$, which is the average energy transferred in deactivating collisions.

The computation of $\alpha = \langle \Delta E_d \rangle$ using our classical trajectory code DiNT[76] involves several steps, and our approach[22,55,67] is similar to approaches used by other groups.[38–41,77] Briefly, the unimolecular reactant A is prepared with a fixed class-dependent initial total energy E' representative of typical dissociation energies (here, 95 kcal/mol for alkanes, 90 kcal/mol for alcohols, and 45 kcal/mol for hydroperoxides) and an initial rotational state J' selected from an independent thermal distribution at the temperature T of interest. As in Ref. 76, vibrationally averaged rotational constants, $\langle B \rangle$ and $\langle A \rangle$, are used to define the thermal populations from which J' is selected. For long linear systems (eg, n-hexadecane), this choice results in significantly different computed values of α (by up to 50%) relative to the less accurate approach of using the equilibrium rotational constants, B_e and A_e. For systems with only a few heavy atoms $\langle B \rangle \approx B_e$, and the two approaches give similar results.

Some additional care must be taken when sampling the internal coordinates of the larger species, as well. We tested several strategies suitable for automation, and, with one exception, we found that our results were insensitive (within our sampling statistics) to the number of different initial low-energy conformers used to initiate the sampling trajectories (we tested using from 1 to 8 conformers) and to the length of the sampling trajectories (which we varied from 25 to 250 ps). The one exception we found is what might be considered the simplest approach. When we used only the linear geometry as the initial structure for the sampling trajectories along with short sampling times, we obtained fairly small (<30%) but statistically significant differences in α relative to the more robust strategies for the largest systems considered here.

The relative collision parameters and any internal coordinates of the bath gas are selected from thermal distributions using standard approaches for bimolecular collisions.[78] The trajectories are propagated classically until A and M are separated enough to unambiguously determine the final state (E,J) of A, from which a variety of energy transfer properties can be computed including $\alpha = \langle \Delta E_d \rangle$. As has been frequently discussed (eg, Refs. 22,23,33,38,77), trajectory calculations (and experiments) necessarily describe *per time* energy transfer averages. One must choose a reference collision rate constant Z to convert this information to the *per collision* averages, like α, that are often of interest. Here we use Z computed using the Lennard-Jones parameters obtained above.

Once the outcomes of an appropriately prepared trajectory ensemble are computed, one can generate any number of different energy and angular-momentum transfer averages as required for parameterizing more detailed higher accuracy models for energy transfer,[22,69] but this is not pursued here. Instead we analyze trends in the single moment α computed for a large number of systems. For each A + M and temperature T, 14 400 trajectories were computed, which for our choices of numerical parameters resulted in 2-sigma Monte Carlo statistical uncertainties in α of ~5%.

Throughout this work, we report trends in $Z n_1 \alpha$ instead of α, where n_1 is the number density of the bath gas at 1 Torr and the temperature of interest. The product $Z\alpha$ describes energy transferred per time and, neglecting angular momentum, is equal to the "deactivating" moment of the collisional energy transfer rate constant that is sometimes written $R(E,E')$, as discussed elsewhere.[18,27] We choose to multiply $Z\alpha$ by n_1 to

give somewhat more manageable units (here, cm^{-1} s^{-1}). This choice of pressure is of no consequence as choosing pressures other than 1 Torr would simply scale all of the results equally. Trends in $Zn_1\alpha$ are often similar to trends in the percollision quantity α, but the former avoids the arbitrariness associated with the particular choice of Z.

2.4 | Data set

A total of 307 unimolecular reactants A with as many as 16 heavy (nonhydrogen) atoms N were considered, including 141 hydrocarbons, 84 alcohols, and 82 hydroperoxides. Results are reported for several series of related systems where N is varied for a fixed branching and oxygen-group functionalization motif. These series are summarized in Tables 1 and 2, which include chemical drawings, and are described next.

The hydrocarbon systems studied here are shown in Table 1. In addition to the series of normal alkanes from methane to hexadecane (N = 1-16), we considered eight series of singly branched methyl- and ethyl- substituted alkanes (eg, the series of 3-ethylalkanes from 3-ethylpentane, N = 7, to 3-ethyltetradecane, N = 16) and eight series of doubly branched dimethyl-substituted alkanes (eg, the series of 2,2-dimethylalkanes from neopentane, N = 5, to 2,2-dimethyltetradecane, N = 16). Four series of highly branched species were considered: a "half methylated" series where every other C atom in the backbone was methyl substituted, a "methylated" series where every C atom in the backbone was methyl substituted, a "dimethylated" series where every C atom in the backbone was dimethyl substituted, and a series representing the "iso" fuels isooctane, isododecane, and isohexadecane.

We considered three series with alkane rings, including cyclopentane and cyclohexane with alkane chain substitutions of various lengths as well as a "polycyclo-" series consisting of cyclohexane, decalin, and the three-ring continuation of the series. Finally, we also considered the aromatic ring versions of the alkane ring series, where we note that the cyclopentadienyl series consists of radicals, unlike all of the other systems considered here.

The oxygenated systems studied here are summarized in Table 2. In addition to the normal alcohol and hydroperoxide series, we considered several series of linear and branched alkanes substituted with one or two hydroxy or peroxy groups, as detailed in Table 2.

2.5 | Automation

Collisional energy transfer parameters for all 307 systems in Tables 1 and 2 were computed at 1000 K and for M = Ar. Additional calculations at T = 300 and 2000 K and for M = He, H$_2$, and N$_2$ were carried out for a subset of these systems. In total, 788 A + M and T combinations were con-

sidered, requiring a total of more than 11 million trajectories. Managing such a large number of computations was aided by the following strategy.

The computation of σ, ε, and α was automated using three levels of codes and scripting.

2.5.1 | Chemical physics codes
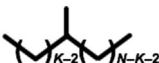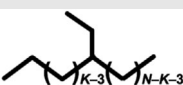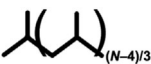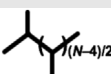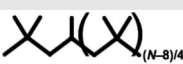
At the lowest level, the chemical physics codes 1DMIN and DiNT read text input files and produce text output files, with the goal of keeping each step at this level as elementary as possible. 1DMIN is inherently simple, for example, requiring only the geometry of A, the identity of M, and the specification of the interaction potential as inputs. The output of 1DMIN is σ and ε. DiNT, on the other hand, has multiple uses, including geometry optimization, initial condition sampling, and trajectory simulations. These steps were carried out independen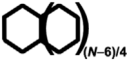tly via separate instances of DiNT, with each step communicating via text inputs and producing different text outputs, as managed at the next level.

2.5.2 | Scripting

The following sequence of elementary chemical physics steps required to generate σ, ε, and α for a single system A + M and temperature T was scripted at the second level. The procedure started with a guessed geometry for A, the identity of the bath gas M, a PES for A + M, and the temperature T. (a) DiNT first optimized the structure of A. (b) 1DMIN read the optimized structure and computed σ and ε. (c) Independently, DiNT read the optimized structure and used it to launch a small number of long-lived trajectories of the isolated molecule A (ie, without M present) designed to sample the internal coordinates and momenta of A microcanonically and subject to class-specific values of the initial energy E'. (d) Vibrationally-averaged rotational constants $\langle B \rangle$ and $\langle A \rangle$ were computed from the geometries generated in step c. (e) The results from steps a, c, and d were read and used by DiNT to set up and run an A + M collisional energy transfer ensemble. (f) The average energy transferred in deactivating collisions for the ensemble in step e was computed and renormalized to the collision rate Z generated from σ and ε computed in step b to produce α.

This stepwise scripting approach has the following useful features. First, intermediate information can be reused; for example, the internal coordinates for A sampled in step c can be reused for other bath gases. Second, the script can be readily restarted and naturally avoids repeating calculations while avoiding complex bookkeeping of the status of the various steps. Instead, each step has a set of input and output files associated with it. The script checks to see if the output file already exists, and, if so, the step is skipped. If the output file does not exist, the script checks for the required input files (which themselves may be output files from other steps). If the

TABLE 1 Series of hydrocarbons

Series	Drawing	M^a	Series[b]	pp|ps|ss	pt|st	tt|tq|qq	pq|sq	ss, ring
n-alkanes		12	$N = 1(1)8,10(2)16$	X				
Singly branched		**39**						
K-methyl-		25	$K = 2(1)4,6,8;$ $N = 2K(1)8,10(2)16$	X	X			
K-ethyl-		14	$K = 3; N = 7,8(2)16$ $K = 4; N = 9,10(2)16$ $K = 6; N = 13,14,16$	X	X			
Doubly branched		**44**						
2,K-dimethyl-		22	$K = 3; N = 6(1)8,10(2)16$ $K = 4; N = 7,8,10(2)16$ $K = 6; N = 9,10(2)16$ $K = 8; N = 11,12(2)16$	X	X	X		
K,K-dimethyl-		22	$K = 2; N = 5(1)8,10(2)16$ $K = 3; N = 7,8(2)16$ $K = 4; N = 9,10(2)16$ $K = 6; N = 13,14,16$	X			X	
Highly branched		**16**						
"half methylated"		4[c]	$N = 7(3)16$		X			
"methylated"		6[c]	$N = 6(2)16$		X	X		
"dimethylated"		3	$N = 8(3)14$			X	X	
"'iso' fuels"		3	$N = 8,12,16$		X		X	
Alkane rings		**16**						
cyclopentyl-		7	$N = 6(1)8,10(2)16$	X	X			X
cyclohexyl-		6	$N = 7,8(2)16$	X	X			X
polycyclo-		3	$N = 6,10,14$	X	X			X
Aromatic rings		**16**						
cyclopenta-dienyl-		7	$N = 6(1)8,10(2)16$	X	X			X
phenyl-		6	$N = 7,8(2)16$	X	X			X
anthracenes		3	$N = 6,10,14$	X	X			X

[a]M is the number of species considered in each group.

[b]The notation $X(Y)Z$ indicates a list from X to Z in steps of Y.

[c]The first member in the series also appears in a dimethyl series.

TABLE 2 Series of alcohols and hydroperoxides

Series	Drawing	M^a	Series[b]	pp|ps|ss	pt|st	tt|tq|qq	pq|sq	CO|O
Alcohols		**84**						
n-alcohols		11	$N = 2(1)9,11(2)15$	X				X
K-ols		24	$K = 2(1)4$; $N = 2K(1)9,11(2)15$ $K = 6;N = 12,13,15$	X	X			X
K,K-diols		23	$K = 2(1)4$; $N = 2K+1(1)10,12(2)16$ $K = 6;N = 13,14,16$	X			X	X
K-methyl-*K*-ols		14	$K = 2,3$; $N = 2K+1(1)9,11(2)15$	X	X	X	X	X
K-methyl-*L*-ols		12	$K = 2;L = 3;N = 7(1)9,11(2)$ $K = 3;L = 2;N = 7(1)9,11(2)$	X	X	X	X	X
Hydroeroxides		**82**						
n-hydroperoxides		10	$N = 3(1)10,12,14$	X				X
K-peroxy-		23	$K = 2;N = 5(1)10,12(2)16$ $K = 3;N = 7(1)9,12(2)16$ $K = 4;N = 9,10(2)16$ $K = 6;N = 13,14,16$	X	X			X
K,K-diperoxy-		23	$K = 2;N = 7(1)14,16$ $K = 3;N = 9(1)14,16$ $K = 4;N = 11(1)14,16$ $K = 6;N = 15,16$	X			X	X
K-methyl-*K*-peroxy-		13	$K = 2; N = 6(1)10,12,14$ $K = 3; N = 8,9,10(2)14$	X	X	X	X	X
K-methyl-*L*-peroxy-		13	$K = 2;L = 3;N = 7(1)9,10(2)16$ $K = 3;L = 2;N = 8,9,10(2)16$	X	X	X	X	X

[a]M is the number of species considered in each group.

[b]The notation $X(Y)Z$ indicates a list from X to Z in steps of Y.

required input files do exist, the job is launched. If not, the step is skipped, presumably because steps involved in generating these files are still running or are yet to be run. The script can be rerun until all input and output files are produced, and all steps are completed. Jobs managed in this way are easily parallelized despite the complex and heterogeneous workflow, particularly when a computational cluster with a queuing system is used.

2.5.3 | Batch processing

At the highest level, simple and trivially parallelized batch scripts were used to loop through desired values of A, M, and T. At this level, one can also implement rules for specifying numerical parameters needed for the calculations, such as the maximum impact parameter, b_{max}, or the center of mass distance used to terminate the trajectory, R_f, which may be system dependent. Here, for example, we generously set $b_{max} = 8$ + $N/2$ Å and $R_f = b_{max} + 3$ Å. Such rules avoid the need for human intervention for each choice of A and allow for the rapid consideration of large numbers of systems. These scripts also collect and tabulate the desired information.

2.6 | Trends

The major goal of the present work is to provide simple rules for estimating the collision parameters σ, ε, and α by studying their dependence on N and the structure of A. These rules are described next. As noted previously[55] and as demonstrated again in Section 3, the Lennard-Jones parameters σ and ε are fairly insensitive to branching and may be well represented for each class of reactants and bath gas as a power law in the number of nonhydrogen ("heavy") atoms N. Power law coefficients and exponents are newly determined here for alcohols

and hydroperoxides, and we update our earlier determinations for hydrocarbons[55] to perform better for large N.

To estimate α, we define an effective number of heavy atoms N_{eff} that is based on the number and type of internal rotors in A. (We are using "rotor" here to mean any bonded pair of heavy atoms, including torsions as well as the constrained rotors appearing in rings.) If both central atoms are C atoms, we label the rotor based on the coordination (p, s, t, and q for primary, secondary, tertiary, or quaternary) of the two central C atoms. For example, propane has two ps rotors, and butane has two ps rotors and one ss rotor. Rotors where one or both of the central atoms is an O atom are counted separately as N_{CO} or N_{OO}. These counts are used to define N_{eff} via

$$
\begin{aligned}
N_{\text{eff}} = 1 &+ c_{\text{pp|ps|ss}}(N_{\text{pp}} + N_{\text{ps}} + N_{\text{ss}}) \\
&+ c_{\text{pt|st}}(N_{\text{pt}} + N_{\text{st}}) \\
&+ c_{\text{pq|sq}}(N_{\text{pq}} + N_{\text{sq}}) \\
&+ c_{\text{tt|tq|qq}}(N_{\text{tt}} + N_{\text{tq}} + N_{\text{qq}}) \\
&+ c_{\text{CO|OO}}(N_{\text{CO}} + N_{\text{OO}}) \\
&+ c_{\text{ss,ring}}N_{\text{ss,ring}} - N_{\text{rings}},
\end{aligned} \tag{1}
$$

where the coefficients c_x scale contributions from the different rotor types, and we have grouped similar rotors together. We distinguish ss rotors appearing in rings from those that do not, and N_{rings} counts rings. When $c_x = 1$ for all x, N_{eff} is equal to the number of heavy atoms N. By choosing $c_x < 1$ for some terms, we show below that N_{eff} maps the computed values of α for branched and oxygenated species onto those for the corresponding normal (linear) series.

The coefficients in Equation (1) may be systematically determined by considering subsets of systems that isolate the dependence of α on certain rotor types. This procedure will be described in Section 3, where we find $c_{\text{pp|ps|ss}} = 1$, $c_{\text{pt|st}} = \frac{2}{3}$, $c_{\text{pq|sq}} = \frac{1}{3}$, $c_{\text{tt|tq|qq}} = 0$, $c_{\text{CO|OO}} = \frac{1}{3}$, and $c_{\text{ss,ring}} = \frac{1}{2}$. Using these parameters, α may be estimated for an unknown system as follows, so long as results for the corresponding normal (linear) series of α are known. We label the linear reference series $\bar{\alpha}$. One first counts rotor types and evaluates N_{eff} via Equation (1), which may be a noninteger number. One may be tempted to estimate α as $\bar{\alpha}(N_{\text{eff}})$ by interpolating nearby values of $\bar{\alpha}$, which of course is known only at integer values of N. Such a procedure would not properly account for changes in the collision rate with N, however. Instead, one should interpolate the product $\overline{Z\alpha}$ for the reference series to determine its value at N_{eff} and then divide by Z for the system size of interest N, that is,

$$
\alpha \approx \overline{Z\alpha}(N_{\text{eff}})/Z(N). \tag{2}
$$

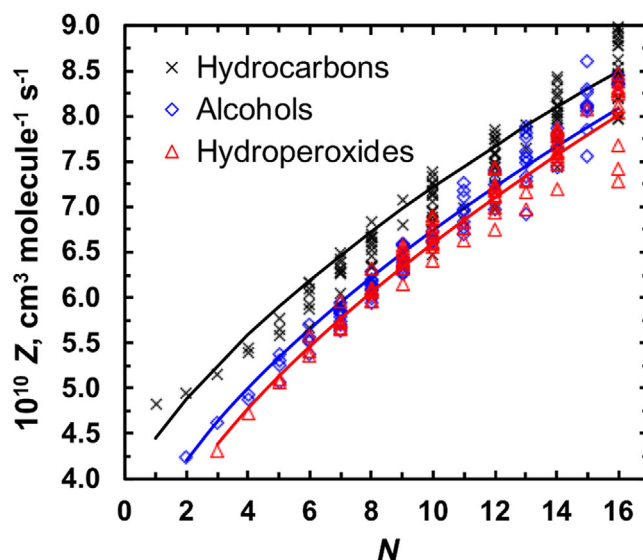**FIGURE 1** Computed Lennard-Jones collision rate constants Z at 1000 K and M = Ar for several hydrocarbons (x), alcohols (diamonds), and hydroperoxides (triangles) and shown as a function of the number of heavy (nonhydrogen) atoms N. Solid lines show the results of the analytic expressions for σ and ε given in the text [Color figure can be viewed at wileyonlinelibrary.com]

An example of this procedure is given at the end of Section 3, and a spreadsheet useful for evaluating Equation (2) is given as the Supporting Information. The Supporting Information also includes results for every system studied here, including all of the useful data appearing in the figures as well as results for temperatures and bath gases mentioned but not presented.

3 | RESULTS AND DISCUSSION

3.1 | Collision rate constants

Lennard-Jones parameters σ and ε were computed for the large set of A + M systems discussed above. Figure 1 shows the results of these calculations for M = Ar converted to Lennard-Jones collision rate constants Z at 1000 K. For a given value of N, the scatter in Z is small enough (typically less than 5%) to neglect for many applications. We therefore express σ and ε as simple functions of N. The results from Figure 1 for M = Ar are well represented by the expressions

$$
\text{hydrocarbons (+Ar)} \quad \sigma(N) = 3.40N^{0.18} \text{ Å}
$$

$$
\varepsilon(N) = 113N^{0.31} \text{cm}^{-1}
$$

$$
\text{alcohols(+Ar)} \quad \sigma(N) = 3.05N^{0.20} \text{ Å}
$$

$$
\varepsilon(N) = 150N^{0.29} \text{cm}^{-1}
$$

$$
\text{hydroperoxides(+Ar)} \quad \sigma(N) = 3.05N^{0.20} \text{ Å}
$$

$$
\varepsilon(N) = 110N^{0.39} \text{cm}^{-1}
$$

where we have improved our previous recommendation for hydrocarbons[55] to better represent $N > 8$. The lines in Figure 1 show the values of Z computed using these expressions. This procedure was repeated for M = He, H_2, and N_2, and we obtained

hydrocarbons(+He) $\sigma(N) = 3.33 N^{0.17}$ Å

$\varepsilon(N) = 21.3 N^{0.31} \text{cm}^{-1}$

hydrocarbons(+H_2) $\sigma(N) = 3.15 N^{0.18}$ Å

$\varepsilon(N) = 75.0 N^{0.30} \text{cm}^{-1}$

hydrocarbons(+N_2) $\sigma(N) = 3.68 N^{0.16}$ Å

$\varepsilon(N) = 100. N^{0.25} \text{cm}^{-1}$

alcohols(+He) $\sigma(N) = 2.90 N^{0.21}$ Å

$\varepsilon(N) = 22.0 N^{0.28} \text{cm}^{-1}$

hydroperoxides(+He) $\sigma(N) = 2.90 N^{0.21}$ Å

$\varepsilon(N) = 10.0 N^{0.75} \text{cm}^{-1}$

3.2 | Tests of the intramolecular potential

Next we briefly consider the sensitivity of the computed values of α to the description of the intramolecular potential. The collision rate constants Z are independent of this choice. Figure 2 shows $Z n_1 \alpha$ computed for the series of n-alkanes in Ar at 1000 K using three molecular mechanics potentials (MM3, AMOEBA09, and OPLSAA) and one semiempirical TB potential. These results are seen to increase nearly linearly with N for small N, they begin to plateau around pentane, and are relatively independent of N for large N. The value of N at which this transition takes place is related to the system size at which the bath gas temperature equals the effective temperature of the internal energy of A.

Results for the three molecular mechanics potentials agree with each other within their 5% 2-sigma statistical sampling uncertainties, whereas results for the TB potential are slightly but systematically lower (by 10%) for alkanes larger than hexane. The TB potential has an unphysical description of torsions, which likely explains this result. The relative insensitivity of collisional energy transfer efficiencies on the description of the intramolecular potential has been noted previously[28,30] and is confirmed again here in this somewhat different context. The MM3 parameterization is used exclusively in the remainder of this work.

3.3 | Lightly branched alkanes

Figure 3 shows $Z n_1 \alpha$ at 1000 K for the alkane series listed in Table 1. In Figure 3A, results for the n-alkanes are compared with those for the series of singly and doubly branched
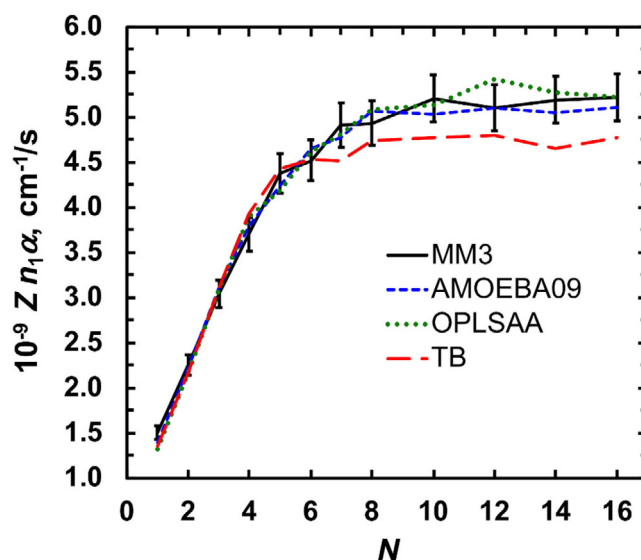

FIGURE 2 The deactivating moment of the energy transfer rate constant $Z\alpha$ multiplied by the number density of the bath gas at 1 Torr n_1 for the series of n-alkanes from methane ($N = 1$) to hexadecane ($N = 16$) computed at 1000 K ($n_1 = 9.7 \times 10^{15}$ 1/cm^3). Results for four intramolecular PESs are shown. The trajectory ensemble sizes used here have 5% 2-sigma statistical uncertainties, as indicated for just one of the curves to reduce clutter [Color figure can be viewed at wileyonlinelibrary.com]

alkanes as a function of N. As in Figure 2, the 2-sigma statistical uncertainties for these results are $\sim$5%, and so we do not attempt to interpret the fine structure of any of these curves. Instead, we note qualitatively that the curves for the singly branched species appear shifted to the right by $\sim$1 heavy atom relative to the n-alkanes, whereas the curves for the doubly branched species appear shifted by $\sim$2 heavy atoms. These qualitative observations were made previously[55] and were the initial motivation for the design of Equation (1).

The parameters in Equation (1) were systematically determined by considering subsets of these data that isolated different rotor types, as marked in Table 1. We first considered the singly branched methyl and ethyl series, which feature pt and st rotor types in addition to ps and ss rotor types found in the n-alkane series. By setting $c_{pp|ps|ss} = 1$ and optimizing the single remaining parameter required to describe these series, $c_{pt|st} = \frac{2}{3}$, we found that the resulting values of N_{eff} closely mapped the K-methylalkane and K-ethylalkane results onto the n-alkane series. Similarly, by considering the 2,3-dimethylalkane series, which features tt rotors, and the K,K-dimethylalkane series, which features pq and sq rotors, we determined $c_{tt|tq|qq} = 0$ and $c_{pq|sq} = \frac{1}{3}$, respectively. Figure 3C shows the results of these three optimizations, where it can be clearly seen that N_{eff} regularizes the results of all 16 branched series (83 systems) to closely match the n-alkane series.

The relationship between N and N_{eff} may be clarified using neopentane as an example, which is the first entry in
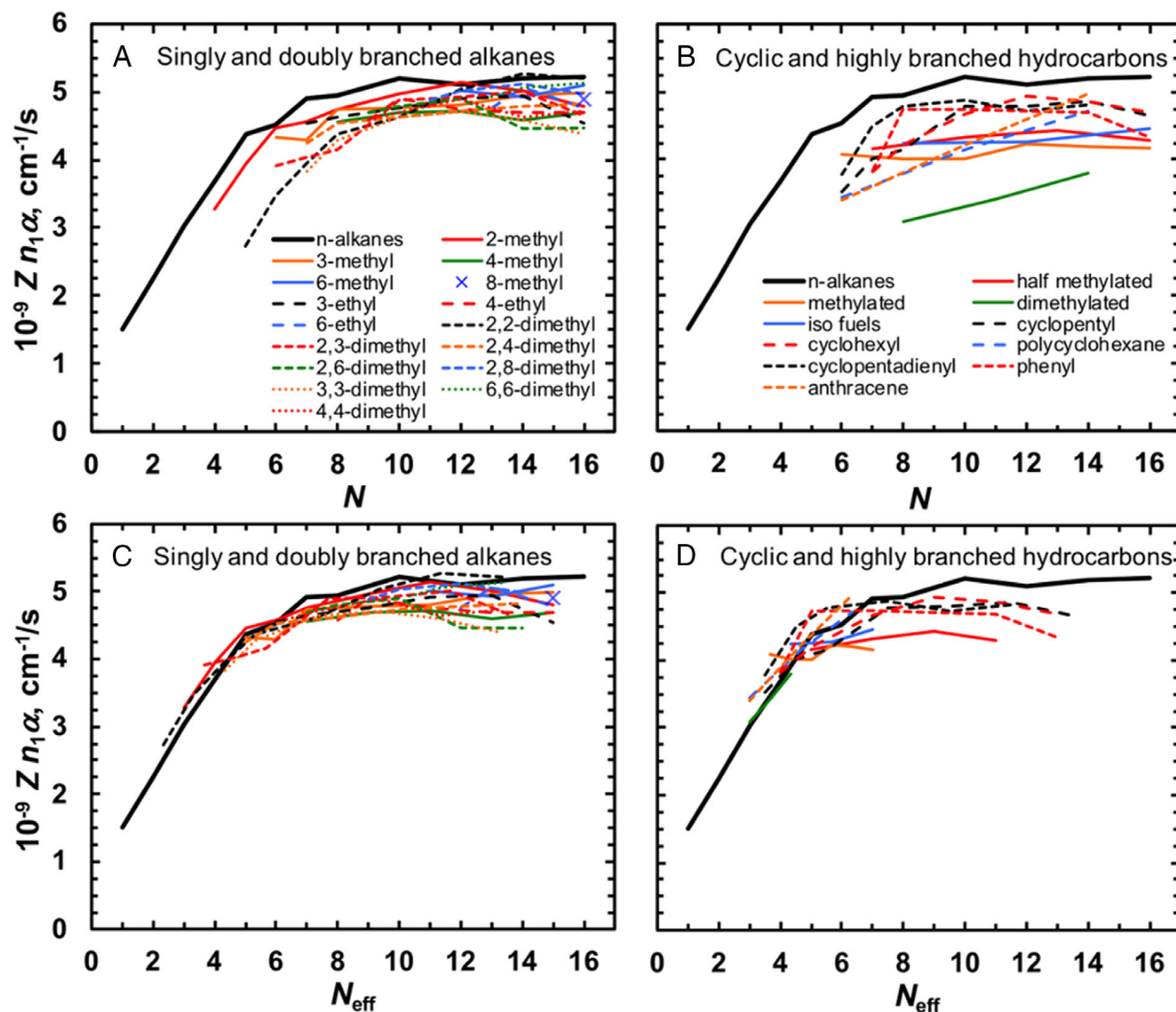
FIGURE 3 $Zn_1\alpha$ for several series of (A,C) singly and doubly branched alkanes and (B,D) cyclic and highly branched alkanes and alkenes at 1000 K. The thick black line shows the results for the normal alkane series. Results are shown in (A,B) as a function of the number of heavy atoms N and again in (C,D) as a function of the effective number of heavy atoms N_{eff} [Color figure can be viewed at wileyonlinelibrary.com]

the 2,2-dimethylalkane series. Its computed collision parameters at 1000 K and for M = Ar are $\alpha = 501$ cm^{-1} and $Z = 5.65 \times 10^{-10}$ cm^3 molecule^{-1} s^{-1}, corresponding to $Zn_1\alpha = 2.73 \times 10^9$ cm^{-1} s^{-1} at 1 Torr Ar, as shown in Figure 3. For this system, $N = 5$, and n-pentane at these same conditions has a similar collision rate ($Z = 5.77 \times 10^{-10}$ cm^3 molecule^{-1} s^1) but a much (∼60%) larger value of $\alpha = 786$ cm^{-1}. According to Equation (1), however, neopentane's four pq rotors give $N_{eff} = 2\frac{1}{3}$, suggesting instead that neopentane should have energy transfer properties more similar to ethane ($\alpha = 473$ cm^{-1}) and propane ($\alpha = 612$ cm^{-1}) than n-pentane, which is in fact the case.

Physically, it appears reasonable to interpret $c_{pp|ps|ss} = 1$ and our empirically optimized values of $c_{pt|st} = \frac{2}{3}$, $c_{pq|sq} = \frac{1}{3}$, and $c_{tt|tq|qq} = 0$ as follows. Rotors involving *only* primary and secondary carbons (as in the pp|ps|ss group) are sufficiently unhindered so as to each contribute equally to energy transfer ($c_{pp|ps|ss} = 1$), on average. Increasing coordination of the C

atoms participating in the rotors leads to more hindrance and evidently less efficient promotion of energy transfer, again, on average. Partially hindered rotors involving just one tertiary carbon atom or just one quaternary carbon atom (as in the pt|st and pq|sq groups) are less efficient but remain active ($c_{pt|st} = \frac{2}{3}$ and $c_{pq|sq} = \frac{1}{3}$), whereas more strongly hindered rotors that involve two tertiary and/or quaternary carbon atoms are not active ($c_{tt|tq|qq} = 0$).

3.4 | Heavily branched alkanes

In Figures 3B and 3D, we test the above determinations of $c_{pp|ps|ss}$, $c_{pt|st}$, and $c_{pq|sq}$ for several highly branched alkanes. As seen in Figure 3B, there is considerable variation in this set of results, which includes strongly hindered species like those in the "dimethylated" and "'iso' fuels" series defined in Table 1. Nonetheless, the three coefficients determined above for the singly and doubly branched species continue to work

well for heavily branched species, as shown in Figure 3D. This result supports the assumption that the rotor corrections are additive, as in Equation (1).

In both Figures 3C and 3D, the dispersion in the results increases for large N_{eff}, suggesting additional errors in the N_{eff} approach for larger systems. The worst performance of Equation (1) in Figure 3D is for the "half methylated" series, where the use of N_{eff} offers little improvement over simply using N to characterize its energy transfer for the largest members of the series. These additional errors may indicate the need for more complicated rules, such as nonadditive rotor (ie, multirotor) corrections and/or finer classifications of rotor types. These strategies were not pursued here, and we simply note that the maximum deviation in the results for large N_{eff} is 20%. We do include a special treatment for rings, however, as discussed next.

3.5 | Rings

Results for three series of species with alkane rings, as described in Table 1, are also shown in Figures 3B and 3D. For these systems, the performance of the coefficients determined above was found to be poor enough that we pursued a special correction for rotors appearing in rings. Such a correction may again be physically motivated by considering the hindrance of the rotors involved, as one expects, for example, ss rotors appearing in rings to be more hindered than ss rotors appearing in linear chains. Empirically, we find that setting $c_{ss,ring} = \frac{1}{2}$ gives values of N_{eff} that are good predictors of collisional energy transfer, as shown in Figure 3D. Note that rings have one "extra" torsion relative to linear alkanes of the same size, which leads to the $-N_{rings}$ term in Equation (1) and thus complicates the interpretation of $c_{ss,ring} = \frac{1}{2}$. Still, it is notable that our empirical optimizations indicate that ss rotors appearing in rings are intermediate in their efficiency in promoting energy transfer relative to the pt|st and pq|sq groups.

3.6 | Cyclic aromatic alkenes

The above tests could be repeated for analogous series of unsaturated systems and radicals, but we do not present such tests here. Instead, we briefly consider three series with aromatic hydrocarbon rings, again as summarized in Table 1, due to the importance of their energy transfer properties controlling molecular growth pathways.[79,80] As shown in Figure 3D, the coefficients optimized for alkanes continue to work well for unsaturated rings, with no special corrections for PAHs, eg, evidently needed.

3.7 | Alcohols and hydroperoxides

Next we consider the 13 series of alcohols and 13 series of hydroperoxides described in Table 2. These series include singly and doubly branched species and some series with two oxygen-containing functional groups (eg, diols). Figures 4A and 4B show the computed values of $Zn_1\alpha$ at 1000 K and 1 Torr Ar for the alcohol and hydroperoxide series, respectively. Relative to the alkane series, the oxygenated systems have lower values of $Zn_1\alpha$ that "plateau" at smaller N, with this behavior appearing more prominently for the hydroperoxides than the alcohols. These trends are consistent with the lower initial internal energies for these groups (90 and 45 kcal/mol for the alcohols and hydroperoxides, respectively) relative the alkanes (95 kcal/mol).

With the alkane coefficients in Equation (1) fixed at the values determined above, we optimized the single remaining parameter $c_{CO|OO} = \frac{1}{3}$ so as to best map the results of the branched and multifunctional oxygenated species onto their respective normal series via N_{eff}. The results of this optimization are shown in Figures 4C and 4D, where the usefulness of using N_{eff} instead of N to predict collisional energy transfer is again clearly demonstrated. The worst performance of the N_{eff} approach in Figure 4 is for the series of diperoxyalkanes, but we note that the maximum dispersion of the results in Figure 4D is still less than 15%.

3.8 | Transferability to other temperatures and other bath gases

A subset of the systems in Figures 3 and 4 was studied at 300 and 2000 K, again for M = Ar. Results at 2000 K are very similar to those for 1000 K in Figures 3 and 4 and are not shown. Figure 5 shows the results of these tests at 300 K for 13 series, where the N_{eff} model is again found to work well. We emphasize that the coefficients in Equation (1) optimized using the 1000 K data were not reoptimized when constructing Figures 5C and 5D. The good performance of N_{eff} in Figures 5C and 5D at 300 K and at 2000 K demonstrates that the coefficients in Equation (1) are indeed transferable to other temperatures, which greatly increases the utility of the approach.

Transferability was tested for the baths M = He, H_2 and N_2, and Figure 6 shows a subset of these tests for alkanes + He and N_2. Results for alcohols and hydroperoxides + He and for alkanes + H_2 are qualitatively similar to those for the alkanes + He and are not shown. The parameterizations determined above for M = Ar are shown to work very well for M = N_2 (Figure 6D), but they are somewhat less accurate for M = He (Figure 6A). It may be of interest to develop bath-specific coefficients for Equation (1), but we do not pursue this here.

3.9 | Estimating the collision parameters σ, ϵ, and α

In this section, we summarize the use of N and N_{eff} to estimate collision parameters. One can trivially compute σ and
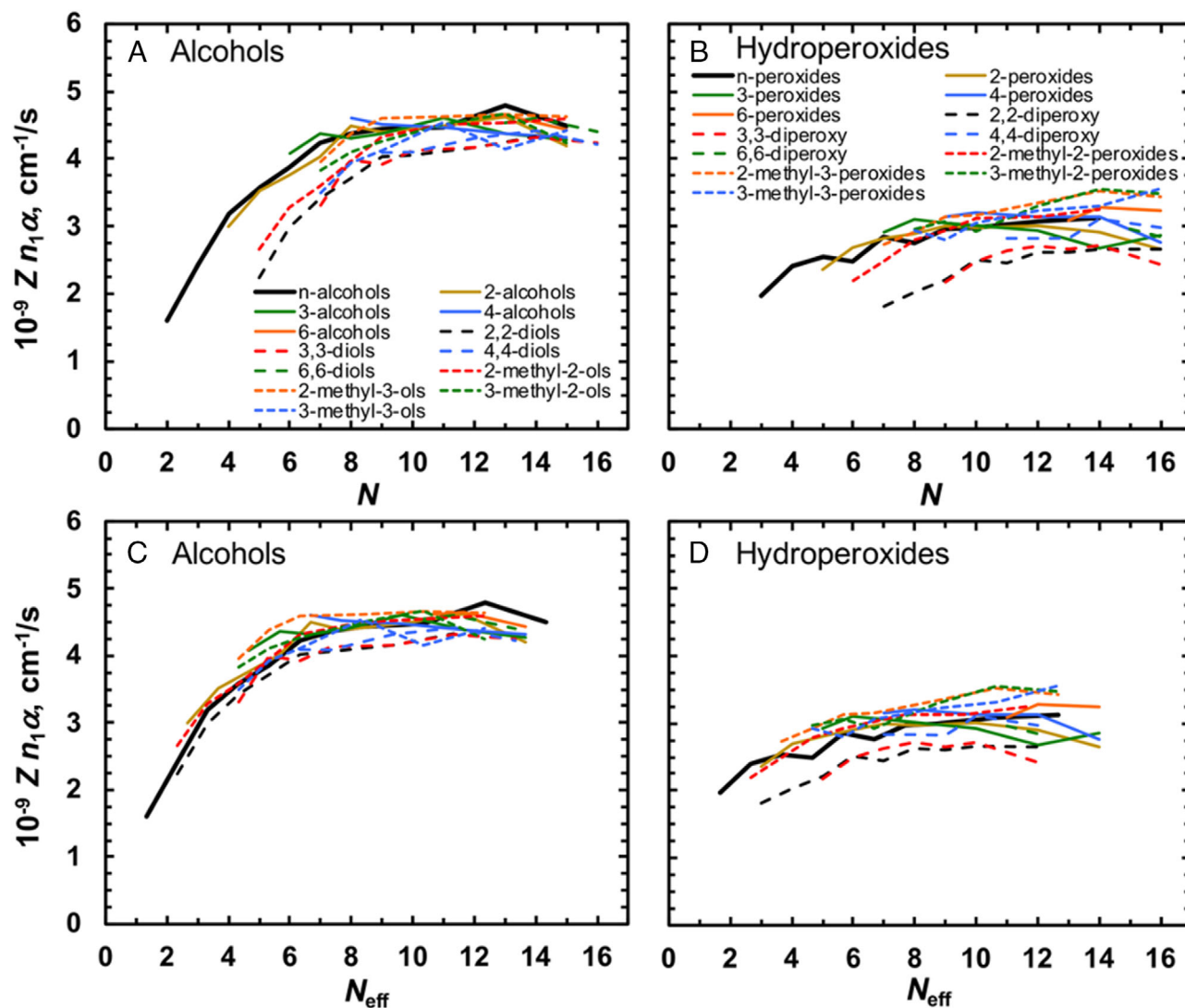
FIGURE 4 $Zn_1\alpha$ for several series of (A,C) alcohols and (B,D) hydroperoxides at 1000 K. Results are shown in (A,B) as a function of the number of heavy atoms N and again in (C,D) as a function of the effective number of heavy atoms N_{eff} [Color figure can be viewed at wileyonlinelibrary.com]

ε for hydrocarbons, alcohols, and hydroperoxides by simply counting the number of nonhydrogen atoms N and using the formulas given at the beginning of this section. We did not consider M = H_2 or N_2 for alcohols and hydroperoxides, but it is likely a good approximation to use assume their values of σ and ε are close to those for M = He or Ar, respectfully, if no better information is available. Similarly, values for M = Ar (or M = N_2, if available) are likely suitable for describing M = Kr, O_2, and CO with sufficient accuracy for many applications. Note also that the collision rates Z for alcohols and hydroperoxides are very similar to one another for a given value of N, and so, again in the absence of better information, it appears reasonable to apply these same formulas to other oxygenated classes of species. Finally, we note that when more accurate values of σ and ε are deemed necessary, one can compute them directly fairly readily using the "one-dimensional minimizations" approach[67] so long as not too many are needed. Higher-accuracy calculations of transport properties are also possible, although these typically require somewhat more computational effort.[16,21]

The direct computation of α requires a nontrivial amount of effort, and a major result from the present work is the strategy for using N_{eff} to avoid this effort. As a demonstration, we consider 2,2,3-trimethylbutane (TMB) + Ar at 1000 K, which was not included in any of the series in Table 1. TMB ($N = 7$) has one tq rotor, two pt rotors, and three pq rotors, such that Equation (1) evaluates to $N_{\text{eff}} = 3\frac{1}{3}$. This value of N_{eff} indicates that TMB's collision properties should be intermediate of propane's ($\bar{\alpha}(3) = 612$ cm^{-1}) and butane's ($\bar{\alpha}(4) = 704$ cm^{-1}). Simply interpolating these values gives 643 cm^{-1}, but as noted in Section 2 such a procedure does not properly account for changes in the collision rate with N.
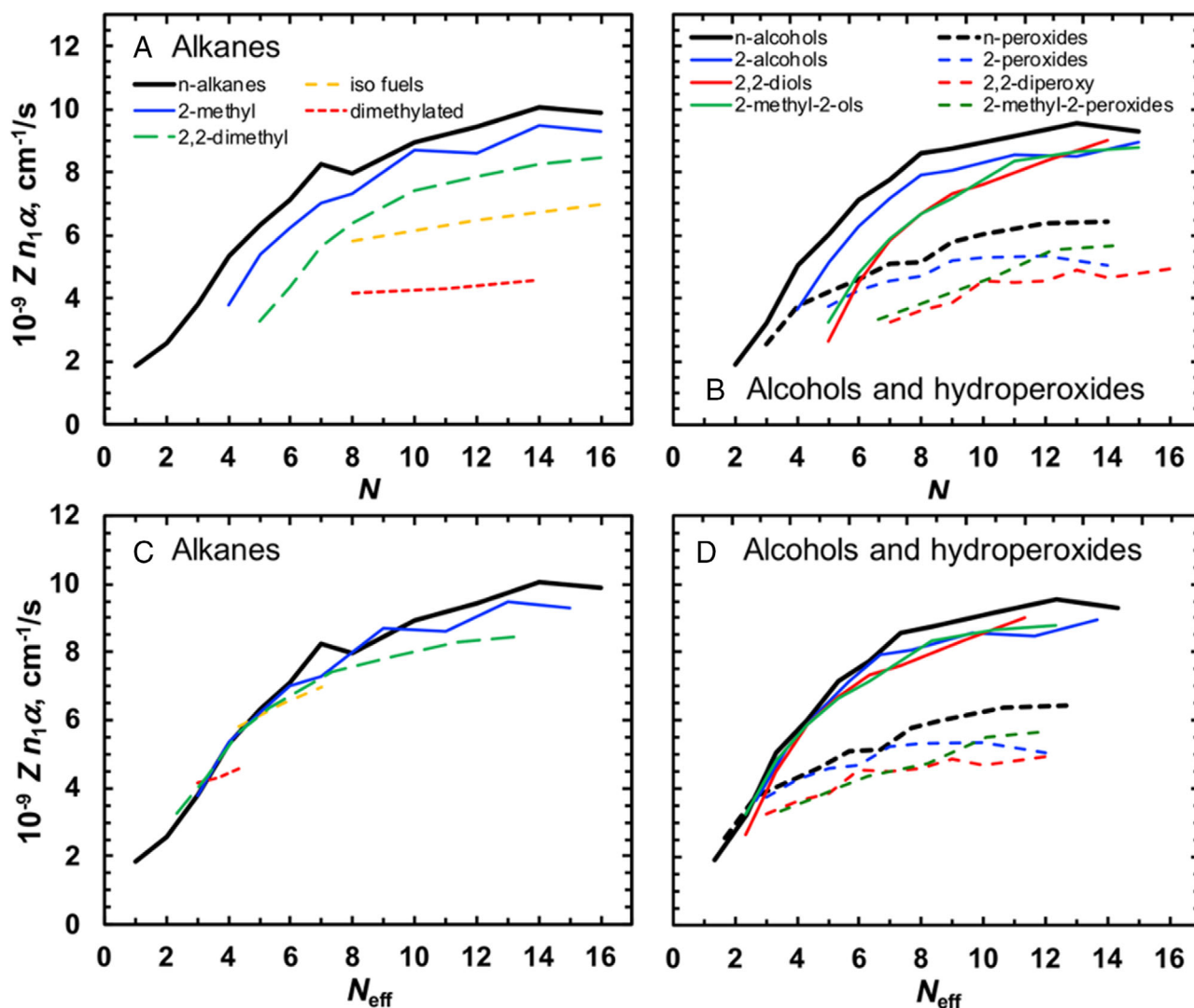
FIGURE 5 $Zn_1\alpha$ at 300 K ($n_1 = 3.2 \times 10^{16}$ 1/cm^3) for (A,C) five series of hydrocarbons and (B,D) eight series of alcohols (solid lines) and hydroperoxides (dashed lines). Results are shown in (A,B) as a function of the number of heavy atoms N and again in (C,D) as a function of the effective number of heavy atoms N_{eff} [Color figure can be viewed at wileyonlinelibrary.com]

Instead, we evaluate Equation (2) for $N_{\text{eff}} = 3\frac{1}{3}$ and $N = 7$ as follows.

For the denominator of Equation (2), $Z(N = 7)$, we could either simply adopt n-heptane's Lennard-Jones parameters ($\sigma = 4.80$ Å and $\varepsilon = 205$ cm^{-1}) and compute Z or else evaluate the expressions given at the beginning of this section ($\sigma = 4.83$ Å and $\varepsilon = 215$ cm^{-1}). These two approaches result in collision rate constants Z that differ by just a few percent. To evaluate the numerator of Eq. (2), we need to interpolate the product $\overline{Z\alpha}$ for $N_{\text{eff}} = 3\frac{1}{3}$. From trajectory calculations, we know that $\overline{Z\alpha}(3) = 315$ and $\overline{Z\alpha}(4) = 383$ for propane and butane + Ar at 1000 K, respectively (in both cases the unwieldy units are 10^9 cm^3 molecule^{-1} s^{-1} cm^{-1}). Linearly interpolating these numbers gives $Z\bar{\alpha}(N_{\text{eff}} = 3\frac{1}{3}) = 338$, which, when divided by 10^9 and the collision rate constant $Z(7) = 6.38 \times 10^{-10}$ cm^3 molecule^{-1} s^{-1}, gives $\alpha \approx 529$ cm^{-1}.

The estimates obtained via this procedure ($\sigma = 4.83$ Å, $\varepsilon = 215$ cm^{-1}, and $\alpha = 529$ cm^{-1}) are in very good agreement ($< 6\%$) with the results of a direct calculation for this system ($\sigma = 4.75$ Å, $\varepsilon = 206$ cm^{-1}, and $\alpha = 560 \pm 28$ cm^{-1}). If we had instead adopted heptane's value of α for TMB, $\bar{\alpha}(7) = 797$ cm^{-1}, our estimate of α would have had an error of $\sim 40\%$.

The use of N_{eff} to estimate α relies on knowing $\overline{Z\alpha}$ for the corresponding normal (linear) series and for the bath gas and temperature of interest. The results calculated here for the normal alkane series + He, Ar, H$_2$, and N$_2$ and for the normal alcohol and hydroperoxides series + He and Ar are given as the Supporting Information, along with analytic formulas fit to these data to aid in the evaluation of Equation (2) for non-integer N_{eff}. If no better information is available, it is likely a good approximation to use the values of α estimated from
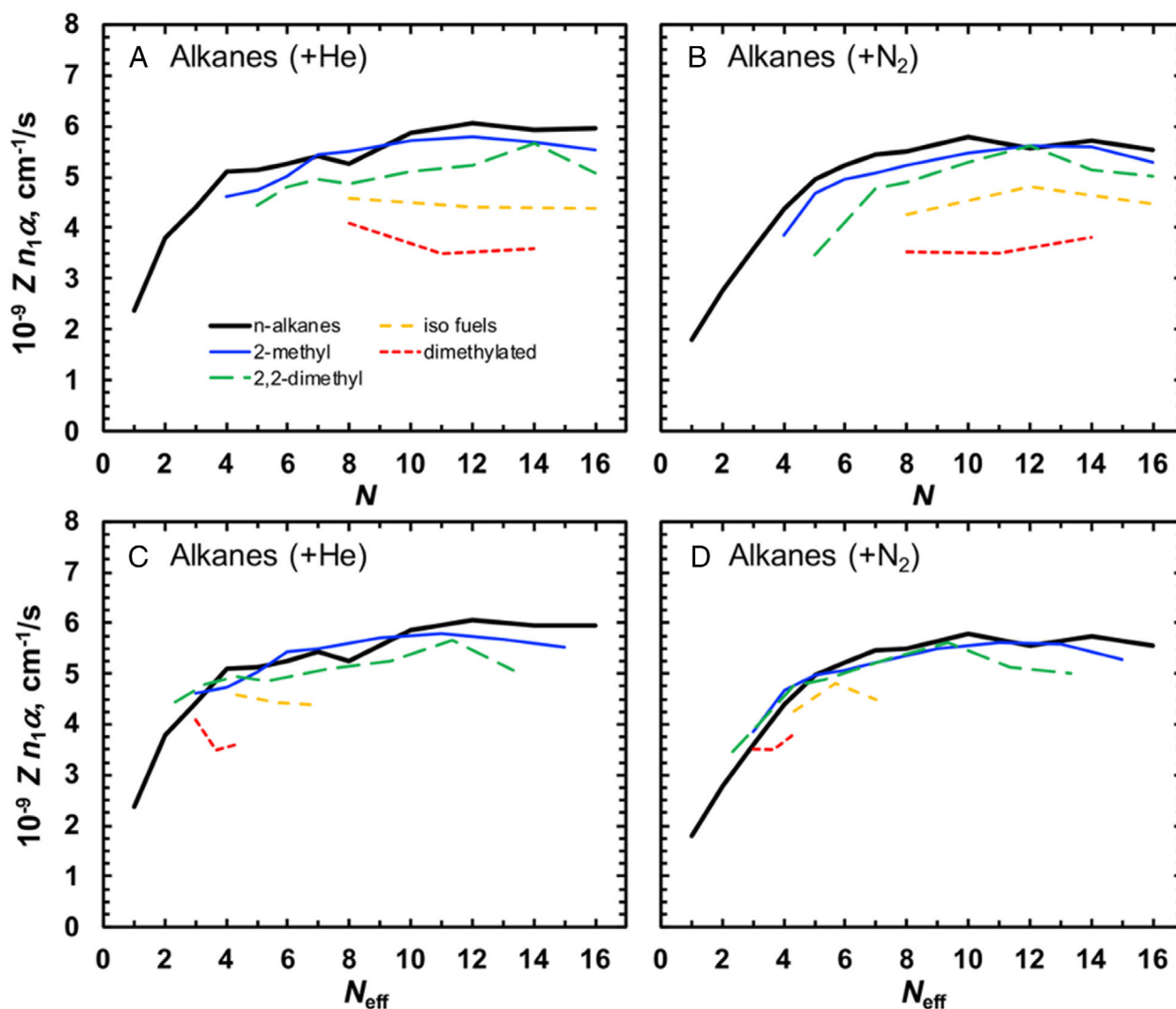
FIGURE 6 $Zn_1\alpha$ for five series of hydrocarbons and (A,C) M = He and (B,D) M = N_2 at 1000 K. Results are shown in (A,B) as a function of the number of heavy atoms N and again in (C,D) as a function of the effective number of heavy atoms N_{eff} [Color figure can be viewed at wileyonlinelibrary.com]

these series for M = Ar or N_2 to describe M = Kr, N_2, O_2, and CO, as these species often have similar energy transfer parameters.

4 | CONCLUSIONS

The computation of Lennard-Jones collision parameters σ and ε and the collision efficiency range parameter α was automated and carried out for 307 alkanes, alcohols, and hydroperoxides, the He, Ar, H_2, and N_2 baths, and at 300, 1000, and 2000 K. This data set was analyzed to develop simple rules for predicting σ and ε based on the type of unimolecular reactant, the number of nonhydrogen atoms N, and the bath gas. For estimating α, we demonstrated the utility of determining an effective number of heavy atoms N_{eff} based on the numbers and types of internal rotors in the system.

The empirical hindering correction parameters that define N_{eff} via Equation (1) were derived and tested using a large data set for M = Ar at 1000 K. We demonstrated the excellent and good transferability of these parameters to other temperatures and bath gases, respectively. This transferability greatly increases the utility of the approach, which should be useful for the rapid estimation of transport parameters and collision efficiencies for large numbers of alcohols, hydroperoxides, and alkanes. This approach is likely readily extended without significant modification to the treatment of more classes of unimolecular reactants A, including unsaturated and radical species. The extension to more bath gases, including strong colliders such as M = H_2O and CO_2, may require further validation of the approach and perhaps specialized bath-specific parameterizations.

Physically, the "effective internal rotor" approach for determining N_{eff}, while empirical, can be readily motivated by

speculating that more strongly hindered rotors, such as those involving tertiary C atoms or appearing in rings, are less efficient at promoting collisional energy transfer, on average, than the relatively unhindered rotors appearing in normal alkanes, alcohols, and hydroperoxides. Closely related explanations based on the size and shape of A, its rotational constants, its vibrational frequencies, and in particular its number of low-frequency vibrations, etc. could also be inferred from these results. It may be of interest to interrogate the results of the trajectories in more detail to further explore these relationships and to provide a more definitive motivation for Equation (1), but we have not done so here.

ACKNOWLEDGMENTS

ORCID

Ahren W. Jasper https://orcid.org/0000-0003-0216-9347

REFERENCES

1. Richter H, Granata S, Green WH, Howard JB. Detailed modeling of PAH and soot formation in a laminar premixed benzene/oxygen/argon low-pressure flame. *Proc Combust Inst*. 2005;30:1397-1405.
2. Davis SG, Joshi AV, Wang H, Egolfopoulos F. An optimized kinetic model of H_2/CO combustion. *Proc Combust Inst*. 2005;30:1283-1292.
3. Sivaramakrishnan R, Brezinsky K, Dayma G, Dagaut P. High pressure effects on the mutual sensitization of the oxidation of NO and CH_4-C_2H_6 blends. *Phys Chem Chem Phys*. 2007;9:4230-4244.
4. Dooley S, Won SH, Chaos M, etal. A jet fuel surrogate formulated by real fuel properties. *Combust Flame*. 2010;157:2333-2339.
5. Mehl M, Pitz WJ, Westbrook CK, Curran HJ. Kinetic modeling of gasoline surrogate components and mixtures under engine conditions. *Proc Combust Inst*. 2011;33:193-200.
6. Kéromnés A, Ketcalfe WK, Heufer KA, etal. An experimental and detailed chemical kinetic modeling study of hydrogen and syngas mixture oxidation at elevated pressures. *Combust Flame*. 2013;160:995-1011.
7. Sarathy SM, Oßwalt P, Hansen N, Kohse-Höinghaus K. Alcohol combustion chemistry. *Prog Energy Combust Sci*. 2014;44:40-102.
8. Curran HJ. Developing detailed chemical kinetic mechanisms for fuel combustion. *Proc Combust Inst*. 2019;37:57-81.
9. Konnov AA. Yet another kinetic mechanism for hydrogen combustion. *Combust Flame*. 2019;203:14-22.
10. Miller JA, Pilling MJ, Troe JJ. Unravelling combustion mechanisms through a quantitative understanding of elementary reactions. *Proc Combust Inst*. 2005;30:43-88.
11. Pilling MJ. From elementary reactions to evaluated chemical mechanisms for combustion models. *Proc Combust Inst*. 2009;32:27-44.
12. Vereecken L, Glowacki DR, Pilling MJ. Theoretical chemical kinetics in tropospheric chemistry: methodologies and applications. *Chem Rev*. 2015;115:4063-4114.
13. Klippenstein SJ. From theoretical reaction dynamics to chemical modeling of combustion. *Proc Combust Inst*. 2017;36:77-111.
14. Mason EA. In Hochstim AR, ed. *Kinetic Processes in Gases and Plasmas*. London: Academic Press; 1969;57-97.
15. Brown NJ, Bastian LAJ, Price PN. Transport properties for combustion modeling. *Prog Energy Combust Sci*. 2011;37:565.
16. Dagdigian PJ. Combustion simulations with accurate transport properties for reactive intermediates. *Combust Flame*. 2015;162:2480.
17. Troe JJ. Theory of thermal unimolecular reactions at low pressures. I. Solutions of the master equation. *Chem Phys*. 1977;66:4745; ibid., 4758.
18. Gilbert RG. Theory of collisional energy transfer of highly excited molecules. *Int Rev Phys Chem*. 1991;10:319-347.
19. Barker JR, Golden DM. Master Equation analysis of pressure-dependent atmospheric reactions. *Chem Rev*. 2003;103:4577.
20. Miller JA, Klippenstein SJ. Master equation methods in gas phase chemical kinetics. *J Phys Chem A*. 2006;110:10528.
21. Jasper AW, Kamarchik E, Miller JA, Klippenstein SJ. First-principles binary diffusion coefficients for H, H_2, and four normal alkanes + N_2. *J Chem Phys*. 2014;141:124313.
22. Jasper AW, Pelzer KM, Kamarchik E, Harding LB, Klippenstein SJ. Predictive a priori pressure-dependent kinetics. *Science*. 2014;346:1212.
23. Brown NJ, Miller JA. Collisional energy transfer in the low-pressure-limit unimolecular dissociation of HO_2. *J Chem Phys*. 1984;80:5568-5580.
24. Schranz HW, Troe J. Trajectory calculations of intermolecular energy transfer in sulfur dioxide-argon collisions. 2. State-specific rate coefficients. *J Phys Chem*. 1986;90:6168-6175.
25. Hu X, Hase WL. Effect of anharmonicity on intermolecular energy transfer from highly vibrationally excited molecules. *J Phys Chem*. 1988;92:4040-4064.
26. Lendvay G, Schatz GC. Observation of highly energetic collisions in classical trajectory studies of collisional energy transfer. *J Phys Chem*. 1990;94:8864-8866.
27. Lim KF, Gilbert RG. Calculation of collisional-energy-transfer rates in highly excited molecules. *J Phys Chem*. 1990;94:72-77.
28. Lendvay G, Schatz GC. Choice of gas kinetic rate coefficients in the vibrational relaxation of highly excited polyatomic molecules. *J Phys Chem*. 1992;96:3752-3756.
29. Lenzer T, Luther K, Troe J, Gilbert RG, Lim KF. Trajectory simulations of collisional energy transfer in highly excited benzene and hexafluorobenzene. *J Chem Phys*. 1995;103:626.
30. Meroueh O, Hase WL. Collisional activation of small peptides. *J Phys Chem A*. 1999;103:3981.
31. Barker JR, Yoder LM, King KD. Vibrational energy transfer modeling of nonequilibrium polyatomic reaction systems. *J Phys Chem A*. 2001;105:796-809.
32. Bernshtein V, Oref I. Collisional energy transfer in polyatomic molecules in the gas phase. *Isr J Chem*. 2007;47:205.

33. Lendvay G. In: Roberton SH, ed. *Unimolecular Kinetics: Parts 2 and 3: Collisional Energy Transfer and the Master Equation*, Vol. 43. Amsterdam, the Netherlands: Elsevier; 2019: 110-272.

34. Hutson JM, McCourt FR. Close-coupling calculations of transport and relaxation cross sections for H_2 in Ar. *J Chem Phys*. 1983;80:1135.

35. Stallcop JR, Partridge H, Walch SP, Levin E. H-N_2 interaction energies, transport cross sections, and collision integrals. *J Chem Phys*. 1992;97:3431.

36. Middha P, Yang B, Wang H. A first-principle calculation of the binary diffusion coefficients pertinent to kinetic modeling of hydrogen/oxygen/helium flames. *Proc Combust Inst*. 2002;29: 1361.

37. Dagdigian PJ, Klos J, Warehime M, Alexander MH. Accurate transport properties for $O(^3P)$-H and $O(^3P)$-H_2. *J Chem Phys*. 2016;145:164309.

38. Barker JR, Weston RE. Collisional energy transfer probability densities P (E, J; E', J') for monatomics colliding with large molecules. *J Phys Chem A*. 2010;114:10619-10633; 2012;116:799(E).

39. Conte R, Houston PL, Bowman JM. Trajectory study of energy transfer and unimolecular dissociation of highly excited allyl with argon. *J Phys Chem A*. 2014;118:7742.

40. Matsugi A. Collision frequency for energy transfer in unimolecular reactions. *J Phys Chem A*. 2018;8:1972-1985.

41. Wang J, Wen K, You X, et al. Energy transfer in intermolecular collisions of polycyclic aromatic hydrocarbons with bath gases He and Ar. *J Chem Phys*. 2019;151:044301.

42. Ahumada JJ, Michael JV, Osborne DT. Pressure dependence and third body effects on the rate constants for $H+O_2$, $H+NO$, and $H+CO$. *J Chem Phys*. 1972;57:3736-3745.

43. Michael JV, Osborne DT, Suess GN. Reaction H+C[sub 2]H[sub 4]: investigation into the effects of pressure, stoichiometry, and the nature of the third body species. *J Chem Phys*. 1973;58: 2800.

44. Michael JV, Payne WA, Whytock DA. Absolute rate constants for $O+NO+M(=He, Ne, Ar, Kr) \rightarrow NO_2+M$ from 217-500 K. *J Chem Phys*. 1976;65:4830-4834.

45. Tardy DC, Rabinovich BS. Intermolecular vibrational energy transfer in thermal unimolecular systems. *Chem Rev*. 1977;77:369-408.

46. Barnes RW, Pratt GL, Wood SW. Pressure dependence of methane dissociation. *J Chem Soc, Faraday Trans*. 1989;85:229-238.

47. Yerram ML, Brenner JD, King KD, Barker JR. Collisional deactivation of highly vibrationally excited benzene pumped at 248 nm. *J Phys Chem*. 1990;94:6341-6350.

48. Feng Y, Niiranen JT, Bencsura A, Knyazev VD, Gutman D. Weak collision effects in the reaction ethyl radical .dblarw. ethene + hydrogen. *J Phys Chem*. 1993;97:871-880.

49. Fletcher FJ, Rabinovitch BS, Watkins KW, Locker DJ. Energy transfer in thermal methyl isocyanide isomerization. Experimental survey 1. *J Phys Chem*. 1996;70:2823-2833.

50. Michael JV, Su M-C, Sutherland JW, Carroll JJ, Wagner AF. Rate constants for $H + O_2 + M \rightarrow HO_2 + M$ in seven bath gases. *J Phys Chem A*. 2002;106:5297-5313.

51. Altinay G, Macdonald RG. Determination of the rate constant for the NH_2 $(X_2 B_1)$ + NH_2 $(X_2 B_1)$ recombination reaction with collision partners He, Ne, Ar, and N_2 at low pressures and 296 K. Part 1. *J Phys Chem A*. 2012;116:1353-1367.

52. Altinay G, Macdonald RG. Determination of the rate constants for the NH_2 (X2 B1) + NH_2 (X2 B1) and NH_2 (X2 B1) + H

53. Shao J, Choudhary R, Susa A, Davidson DF, Hanson RK. Shock tube study of the rate constants for $H + O_2 + M \rightarrow HO_2 + M$ (M = Ar, H_2O, CO_2, N_2) at elevated pressures. *Proc Combust Inst*. 2019;37:145-152.

54. Choudhary R, Girard JJ, Shao J, Davidson DF, Hanson RK. Measurement of the reaction rate of H+O-2+M->HO2+M, for M= Ar, N-2, CO2, at high temperature with a sensitive OH absorption diagnostic. *Combust Flame*. 2019;203:265-278.

55. Jasper AW, Oana CM, Miller JA. "Third-body" collision efficiencies for combustion modeling: hydrocarbons in atomic and diatomic baths. *Proc Combust Inst*. 2015;35:197-204.

56. Jasper AW, Davis MJ. Parameterization strategies for intermolecular potentials for predicting trajectory-based collision parameters. *J Phys Chem A*. 2019;123:3464-3480.

57. Jasper AW, Miller JA. Theoretical Unimolecular kinetics for $CH_4 + M \overset{\rightarrow}{\leftarrow} CH_3 + H + M$ in eight baths, M = He, Ne, Ar, Kr, H_2, N_2, CO, and CH_4. *J Phys Chem A*. 2011;115:6438-6455.

58. Stace AJ, Murrell JN. A classical trajectory study of collisional energy transfer in thermal unimolecular reactions. *J Chem Phys*. 1978;68:3028-3039.

59. Gallucci CR, Schatz GC. Energy transfer, stabilization, and dissociation in collisions of helium with highly excited hydroperoxo. *J Phys Chem*. 1982;86:2352-2358.

60. Yan T, Hase WL. Comparisons of models for simulating energy transfer in Ne-atom collisions with an alkyl thiolate self-assembled monolayer ±. *J Phys Chem B*. 2002;106:8029-8037.

61. Majumder M, Gibson KD, Sibener SJ, Hase WL. Chemical dynamics simulations and scattering experiments for O_2 collisions with graphite. *J Phys Chem C*. 2018;122:16048-16059.

62. Ponder JW. *TINKER – Software Tools for Molecular Design*. . St. Louis, MO: Washington University Medical School; 2017. Version 7.1.2.

63. Allinger NL, Yuh YH, Lii JH. Molecular mechanics. The MM3 force field for hydrocarbons. 1. *J Am Chem Soc*. 1989;111:8551-8566.

64. Cornell WD, Cieplak P, Bayly CI, et al. A second generation force field for the simulation of proteins, nucleic acids, and organic molecules. *J Am Chem Soc*. 1995;117:5179-5197.

65. Jorgensen WL, Maxwell DS, Tirado-Rives J. Development and testing of the OPLS all-atom force field on conformational energetics and properties of organic liquids. *J Am Chem Soc*. 1996;118:11225-11236.

66. Wang Y, Mak CH. Transferable tight-bonding potential for hydrocarbons. *Chem Phys Lett*. 1995;235:37-46.

67. Jasper AW, Miller JA. Lennard-Jones parameters for combustion and chemical kinetics modeling from full-dimensional intermolecular potentials. *Combust Flame*. 2014;161:101-110.

68. Jasper AW, Miller JA, OneDMin: A code for calculating Lennard-Jones parameters from detailed intermolecular potentials via one-dimensional minimizations, July 2014. https://tcg.cse.anl.gov/papr/codes/onedmin.html.

69. Jasper AW. Microcanonical rate constants for unimolecular reactions in the low-pressure limit. *J Phys Chem A*. 2020;124:1205-1226.

70. Barker JR, Golden DM. Master equation analysis of pressure-dependent atmospheric reactions. *Chem Rev*. 2003;103:4577-4591.

71. Pilling MJ, Robertson SH. Master equation models for chemical reactions of importance in combustion. *Annu Rev Phys Chem*. 2003;54:245-275.

72. Miller JA, Klippenstein SJ. Master equation methods in gas phase chemical kinetics. *J Phys Chem A*. 2006;110:10528-10544.

73. Jasper AW, Miller JA, Klippenstein SJ. Collision efficiency of water in the unimolecular reaction CH_4 ($+H_2O$) $\overset{\leftarrow}{\rightarrow}$ CH_3 + H ($+H_2O$): one-dimensional and two-dimensional solutions of the low-pressure-limit master equation. *J Phys Chem A*. 2013;117:12243-12255.

74. Tranter RS, Jasper AW, Randazzo JB, Lockhart JPA, Porterfield, JP. Recombination and dissociation of 2-methyl allyl radicals: experiment and theory. *Proc Combust Inst*. 2017;36:211-218.

75. Jasper AW, Miller JA. Collisional energy transfer in unimolecular reactions: direct classical trajectories for $CH_4 \leftrightarrow CH_3$ + H in helium. *J Phys Chem A*. 2009;113:5612-5619.

76. Jasper AW, Oana CM, Truhlar DG, DiNT: direct nonadiabatic trajectories, July 2013. https://tcg.cse.anl.gov/papr/codes/dint.html.

77. Lim KF, Gilbert RG. Calculation of collisional-energy-transfer rates in highly excited molecules. *J Phys Chem*. 1990;94:72-77.

78. Truhlar DG, Muckerman JT. In: Bernstein RB, ed. *Atom-Molecule Collision Theory: A Guide for the Experimentalist*. New York, NY: Plenum Press; 1979:505-566.

79. Mebel AM, Georgievskii Y, Jasper AW, Klippenstein SJ. Pressure-dependent rate constants for PAH growth: formation of indene and its conversion to naphthalene. *Faraday Discuss, Chem Soc*. 2016;195:637-670.

80. Mebel AM, Georgievskii Y, Jasper AW, Klippenstein SJ. Temperature- and pressure-dependent rate coefficients for the HACA pathways from benzene to naphthalene. *Proc Combust Inst*. 2017;36:919-926.

SUPPORTING INFORMATION

Additional supporting information may be found online in the Supporting Information section at the end of the article.